JCTC Journal of Chemical Theory and Computation

Article

pubs.acs.org/JCTC

Alchemical Free Energy Differences in Flexible Molecules from Thermodynamic Integration or Free Energy Perturbation Combined with Driven Adiabatic Dynamics

Michel A. Cuendet and Mark E. Tuckerman*

Department of Chemistry, New York University, New York, New York 10003, United States

Supporting Information

ABSTRACT: Alchemical free energy simulations are commonly used to calculate relative binding or solvation free energies in molecular systems. The convergence of alchemical free energy calculations is often hampered by inefficient sampling of the conformational degrees of freedom, which remain trapped in metastable substates. Here, we show that thermodynamic integration (TI) or free energy perturbation (FEP) can be combined with the recent driven adiabatic free energy dynamics (dAFED) method, in order to enhance conformational sampling along a set of chosen collective variables. The resulting TI-dAFED or FEP-dAFED methods are validated on a two-dimensional analytical problem. The ability of these methods to provide accurate free energy differences for realistic molecular systems is demonstrated by calculating the enantiomerization free energy of the alanine dipeptide in explicit solvent.

INTRODUCTION

Calculating free energy differences has been one of the central goals of molecular simulation since the inception of the discipline.[1,2] Free energy calculations are mainly applied to two categories of problems: (1) the free energy difference between metastable conformations of a given system, in processes such as the folding of a polypeptide chain or the binding of a drug to its target, and (2) the free energy difference between various systems for a given process such as solvation, ligand binding, or point mutations in proteins. For the second category, computer simulation offers the ability to perform nonphysical (alchemical) transformations from one compound into another. It has long been recognized[3] that following such alchemical paths is much more efficient for calculating free energy differences than simulating the actual solvation or binding process for each compound. Alchemical transformations are usually described with an order parameter λ interpolating the potential energy functions of the two systems. Since the free energy is a state function, the functional form of the interpolation, or λ path, is arbitrary.

The traditional alchemical free energy methods are thermodynamic integration (TI)[4] and free energy perturbation (FEP).[5] Calculations based on these methods have been extensively studied and elaborated upon.[6−8] One of the key limitations previously identified in early free energy simulations[9,10] is the problem of conformational sampling. Free energy calculations utilizing straightforward molecular dynamics (MD) simulations suffer from slow exploration along many conformational degrees of freedom, which hampers the convergence of the free energy estimates. In particular, protein conformational changes, even at the side chain rotamer level, can happen on time scales longer than a typical MD simulation. Further examples include ligands with multiple binding modes whose interconversion is hindered by large kinetic barriers, or water molecules trapped in binding pockets that exchange very slowly with the solvent bulk. Finally, large and flexible ligands such as peptides can be very disordered in solution, complicating the computation of free energy differences in the unbound state. In all of these cases, failure to adequately sample the conformational space will impact the accuracy of free energy calculations.

These challenges prompted several recent efforts to combine enhanced conformational sampling techniques with alchemical free energy methods. The resulting approaches fall into three groups based on the way enhanced sampling is induced: by running independent trajectories, by acting on λ, or by acting on atomic coordinates directly.

Approaches of the first group entail running independent TI or FEP simulations in separate conformational substates and averaging the resulting contributions. For example, the independent trajectory thermodynamic integration (IT-TI) method[11,12] averages (without weighting) TI results from randomly seeded trajectories. The use of multiple independent trajectories was also shown to accelerate convergence in the context of the single-step perturbation technique.[13] Alternatively, if significant conformational substates can be identified beforehand, one can run separate TI simulations restrained to each substate,[9,14] with the extra requirement of calculating the confinement free energy. In the locally enhanced sampling method,[15] noninteracting copies of a relevant part of the system are simulated simultaneously in different conformations and treated in a mean-field fashion.

The second group of approaches is based on varying the λ parameter during the simulation to help the system overcome barriers between conformational substates. One popular family of such approaches is based on the Hamiltonian replica exchange method (HREM), which use λ swaps between

Special Issue: Wilfred F. van Gunsteren Festschrift

Received: February 1, 2012

   dx.doi.org/10.1021/ct300090z | J. Chem. Theory Comput. XXXX, XXX, XXX−XXX

simulations with neighboring λ values. In the replica exchange thermodynamic integration (RETI)[16] method by Woods et al., the standard TI protocol is combined with HREM to improve conformational sampling. The Yang group showed that using a dual topology scheme together with HREM can improve sampling even more[17,18] because the uncoupled copy of the system can freely overcome barriers. HREM was also combined with FEP by Meng et al.,[19] as well as Roux and co-workers,[20] who later proposed a more elaborate version of the method including boosting potentials.[21] A different family of methods called λ dynamics[22−24] enforces variations of λ by considering it as an extended dynamical variable, whose sampling can be enhanced in various ways. The original λ-dynamics method[22] uses umbrella sampling.[25] In λ-AFED[26] (related to the present method, see below), λ is adiabatically decoupled from the physical degrees of freedom and coupled to a high-temperature heat bath. In the recent λ-metadynamics[27] method, an adaptive bias potential acts on λ to overcome free energy barriers.

In the third group of approaches, enhanced sampling is applied directly to the conformational degrees of freedom of the system. For example, one can use bias potentials to enhance conformational sampling, together with an appropriate unbiasing procedure to recover correct ensemble averages for TI or FEP. The idea of using of an umbrella potential to bias a TI or FEP simulation goes back to the work of Tobias[10] et al. More recently, Leitgeb[28] et al. proposed the non-Boltzmann TI (NBTI) approach based on adaptive umbrella sampling. Alternatively, one can alter the original potential energy function to lower barriers. In the enhanced sampling one-step perturbation method,[29] conformational sampling is accelerated by using a reference Hamiltonian smoothed with soft-core potentials,[30] based on which the relative binding free energy of a family of ligands is estimated via single-step FEP. The McCammon group has recently shown that TI can also be combined with the powerful accelerated MD method,[31] in which boost potentials are applied to the energy landscape by either filling up wells or flattening barriers.

In the present paper, we introduce a method belonging to the third group, which uses temperature accelerated molecular dynamics (TAMD),[32] also known as driven adiabatic free energy dynamics (dAFED),[33] to help the system overcome configurational barriers in free energy calculations. The method relies on defining a few collective variables (CVs) that describe important transitions between conformational substates of the system of interest. Each CV is coupled to an additional dynamical variable evolving together with the physical degrees of freedom. These extended variables are assigned large fictitious masses, which yields very different time scales in the physical and extended systems, and reduced heat transfer between them. The resulting adiabatic separation allows the extended variables to be simulated at high temperature, which effectively drives the CVs over free energy barriers and enhances sampling in the physical system. The free energy surface in the CV space can then be recovered directly from the sampled histogram or from the thermodynamic force.[34]

In the following, we first review the TAMD/dAFED method and show how the ensemble average of an observable can be obtained from a TAMD/dAFED simulation. This provides the theoretical foundation for the TI-dAFED and FEP-dAFED methods. We proceed by validating our theoretical results on a two-dimensional problem with an analytical solution. Next, we demonstrate the applicability of TI-dAFED and FEP-dAFED to a molecular system in explicit solvent. We calculate the free energy variation for the enantiomerization of the alanine dipeptide, for which the result is known *a priori*.

METHODOLOGY

The TAMD/dAFED Method. The TAMD/dAFED method is an improvement over the earlier Adiabatic Free Energy Dynamics (AFED) method[36−38] (see also ref 39), which worked directly in the CV space and, therefore, required cumbersome coordinate transformations. Consider a physical system composed of N particles described by the $3N$-dimensional vectors of coordinates r and momenta p. The evolution is governed by the Hamiltonian, $H(p,r) = K(p) + V(r)$, where $V(r)$ is the potential energy function and $K(p) = p^T M^{-1} p/2$ is the kinetic energy, with M a diagonal mass matrix. In order to describe the process of interest, we define a set of n CVs, $q(r)$: $\mathbb{R}^{3N} \rightarrow \mathbb{R}^n$, with $n \ll 3N$. Each CV, itself, is assumed to be a scalar function. In the following, we explicitly write only the configurational part of phase space integrals and denote the ideal gas contribution of the momenta p at inverse temperature $\beta = 1/k_B T$ with $\Lambda_p(\beta)$. Accordingly, the partition function of the physical system is defined as

$$Q_\beta = \Lambda_p(\beta) \int \mathrm{d}r\ \mathrm{e}^{-\beta V(r)} \tag{1}$$

We are interested in the n-dimensional potential of mean force (PMF), $\phi_\beta(s)$, which describes the free energy of the system at temperature T for a given value of the CV, $q(r) = s$, with $s \equiv (s_1,...,s_n)$. The PMF $\phi_\beta(s)$ and the associated probability density $\rho_\beta(s)$ are defined by

$$\rho_\beta(s) \propto \mathrm{e}^{-\beta\phi_\beta(s)} = \int \mathrm{d}r\ \delta^{(n)}(q(r) - s)\ \mathrm{e}^{-\beta V(r)} \tag{2}$$

Each component of the Dirac δ function in eq 2 can be written as the limit of a Gaussian

$$\delta(q_i(r) - s_i) = \lim_{k_i \rightarrow \infty} \sqrt{\frac{\beta k_i}{2\pi}}\ \mathrm{e}^{-\beta \frac{k_i}{2}[q_i(r) - s_i]^2} \tag{3}$$

With this, the PMF takes the form

$$\mathrm{e}^{-\beta\phi_\beta(s)} = \lim_{k \rightarrow \infty} C(k) \int \mathrm{d}r\ \mathrm{e}^{-\beta[V(r) + \sum_{i=1}^{n} \frac{k_i}{2}[q_i(r) - s_i]^2]} \tag{4}$$

The integrand in this expression can be seen as the canonical distribution of an extended dynamical system with coordinates (r,s) subjected to a modified potential energy function $\tilde{V}(r, s) = V(r) + \sum_i (k_i/2)(q_i(r) - s_i)^2$. In this picture, s_i is no longer a parameter but is considered as an additional dynamical variable with momentum p_{s_i} and mass m_{s_i} that is coupled to $q_i(r)$ via the harmonic constant k_i. The evolution is directed by the extended Hamiltonian $\tilde{H}(p, p_s, r, s) = K(p) + K(p_s) + \tilde{V}(r, s)$, where we have defined $p_s \equiv (p_{s_1},...,p_{s_n})$ and the corresponding kinetic energy $K(p_s)$. To simplify the notation, we write m_s and k for all $i = 1,...,n$, but we must keep in mind that these parameters can take different numerical values (especially when CVs have different units).

The mass m_s parameters appear in the extended partition function only in the ideal gas term $\Lambda_{p_s}(\beta)$ and are thus arbitrary. If the m_s paramerters are all taken to be much larger than typical masses in the physical system, the evolution of the s variable will be very slow. In this case, the s variable will evolve on the effective potential created by the averaged fluctuations of the physical system, which is the PMF, eq 4, in the limit $k \rightarrow$

dx.doi.org/10.1021/ct300090z | J. Chem. Theory Comput. XXXX, XXX, XXX−XXX

∞. We can write the approximate PMF for finite k (up to a constant independent of β) as

$$\tilde{\phi}_\beta(s) = -\frac{1}{\beta}\ln\left[\int \mathrm{d}r\ \mathrm{e}^{-\beta\tilde{V}(r,s)}\right] \tag{5}$$

Thus, the extended system will evolve according to the effective Hamiltonian $H_{\mathrm{adb}}(p_s,s) = K(p_s) + \tilde{\phi}_\beta(s)$. If the mass ratio m_s/m is large enough, the time scales of the motions of r and s will be such that no heat (or work) will be exchanged between the physical and extended systems. If this adiabatic separation is effective, we are free to couple the extended system to a heat bath at a temperature T_s higher than T. Doing so allows the CVs to cross high barriers more readily, thereby enhancing the sampling. In this case, the ensemble of the extended system is described by the partition function

$$Q_{\mathrm{adb}}(\beta_s) = \Lambda_{p_s}(\beta_s)\int \mathrm{d}s\ \mathrm{e}^{-\beta_s\tilde{\phi}_\beta(s)} \tag{6}$$

The integrand in eq 6 represents the probability of observing the system at position s during an adiabatic simulation, $\rho_{\mathrm{adb}}(s) \propto \mathrm{e}^{-\beta_s\tilde{\phi}_\beta(s)}$. It follows that the potential of mean force of the physical system (at inverse temperature β) can be obtained from a simulation of the extended system with the s variable at inverse temperature β_s

$$\tilde{\phi}_\beta(s) = -\frac{1}{\beta_s}\ln[\rho_{\mathrm{adb}}(s)] + C \tag{7}$$

This will be a good approximation of the true PMF $\phi_\beta(s)$ provided two assumptions hold. First, k must be large because $\phi_\beta(s) = \lim_{k\to\infty}\tilde{\phi}_\beta(s)$. Second, m_s must be large enough to ensure an effective adiabatic decoupling between physical and extended degrees of freedom. Note that if there are degeneracies, i.e., disjoint conformations r that satisfy $q(r) \approx s$ but can interconvert only for $q(r) \neq s$, the apparent PMF during a single passage at s will not strictly be $\tilde{\phi}_\beta(s)$. However, after many passages, the final observed $\rho_{\mathrm{adb}}(s)$ reflects the true PMF. This is confirmed by the asymptotic analyses of the dAFED dynamics found in refs 32 and 34 based on a perturbation expansion of the density of states, which does not rely on local properties along the trajectory.

It was shown in recent developments of the TAMD/dAFED method[34,35] that the PMF $\tilde{\phi}_\beta(s)$ can alternatively be reconstructed from the mean force instead of the histogram $\rho_{\mathrm{adb}}(s)$. By definition, the mean force is the negative derivative of the PMF:

$$\mathcal{F}(s) = -\nabla_s\tilde{\phi}_\beta(s) \tag{8}$$

$$= \frac{1}{\tilde{Z}_\beta(s)}\int \mathrm{d}r\ k(q(r) - s)\ \mathrm{e}^{-\beta\tilde{V}(r,s)} \tag{9}$$

$$= \langle f\rangle_r(s) \tag{10}$$

In the second line, we have used the definition of the PMF, eq 5. Accordingly, the normalization factor is $\tilde{Z}_\beta(s) = \mathrm{e}^{-\beta\tilde{\phi}_\beta(s)}$. In the last line, we have defined the force $f(r,s) = k(q(r) - s)$ exerted by the physical system on the extended variable s. Here and in the following, $\langle\cdot\rangle_r(s)$ denotes an ensemble average over r only with the value of s fixed. Note the similarity of the above expressions to the TI method.

It was shown in ref 34 that, under adiabatic conditions, the mean force is not affected by the actual distribution of s. In particular, this distribution can be chosen as a canonical distribution at arbitrary temperature T_s, as in eq 6. It follows that if the mean force $\mathcal{F}(s)$ is accumulated in bins during a dAFED simulation, the PMF can be obtained by numerical integration of $\mathcal{F}(s)$

$$\tilde{\phi}_\beta(s) = \int \mathrm{d}s\ \langle f\rangle_r(s) + C \tag{11}$$

Note that the numerical integration in eq 11 requires $\langle f\rangle_r(s)$ to be a consistent multidimensional gradient, which will not be strictly true for simulation data, due to statistical noise. The PMF can however easily be reconstructed as the surface whose discrete derivative best fits $\mathcal{F}(s)$ in the least-squares sense. This postprocessing step provides the additional benefit of producing a smooth PMF.

Ensemble Average of an Observable from TAMD/dAFED Dynamics. The partition function for the extended system at inverse temperature β is

$$\tilde{Z}_\beta = \int \mathrm{d}s\int \mathrm{d}r\ \mathrm{e}^{-\beta\tilde{V}(r,s)} = \int \mathrm{d}s\ \mathrm{e}^{-\beta\tilde{\phi}_\beta(s)} \tag{12}$$

where we have used the definition of the PMF, eq 5. The average of an observable $A(r)$ in the corresponding ensemble is defined as

$$\langle A\rangle = \frac{1}{\tilde{Z}_\beta}\int \mathrm{d}s\int \mathrm{d}r\ A(r)\ \mathrm{e}^{-\beta\tilde{V}(r,s)} \tag{13}$$

In addition, we can define the average of A for a fixed value of the extended variable s

$$\langle A\rangle_r(s) = \frac{1}{\tilde{Z}_\beta(s)}\int \mathrm{d}r\ A(r)\ \mathrm{e}^{-\beta\tilde{V}(r,s)} \tag{14}$$

Using this definition together with eq 5 to express the denominator in terms of the PMF, we can write

$$\int \mathrm{d}r\ A(r)\ \mathrm{e}^{-\beta\tilde{V}(r,s)} = \langle A\rangle_r(s)\ \mathrm{e}^{-\beta\tilde{\phi}_\beta(s)} \tag{15}$$

Under adiabatic conditions, the evolution of s is slow enough to assume that $\langle A\rangle(s)$ can converge for a small interval in s. Assuming this, we can consider the variable s to be fixed in eq 15 and insert this expression, together with eq 12, into the definition 13 of the ensemble average

$$\langle A\rangle = \frac{\int \mathrm{d}s\ \langle A\rangle_r(s)\ \mathrm{e}^{-\beta\tilde{\phi}_\beta(s)}}{\int \mathrm{d}s\ \mathrm{e}^{-\beta\tilde{\phi}_\beta(s)}} \tag{16}$$

If the adiabatic separation is effective, we can raise the temperature of the extended variable to T_s and sample $\langle A\rangle_r(s)$ in small bins of s. During the same simulation, we can sample a histogram of s and use eq 7 to estimate the PMF on the same bins. Alternatively, the PMF can be reconstructed from the mean force using eq 11. With $\langle A\rangle_r(s)$ and $\tilde{\phi}_\beta(s)$, we can reconstruct the overall average $\langle A\rangle$ of our observable at inverse temperature β *a posteriori* by numerically integrating eq 16.

Going one step further, we can ask whether one could obtain $\langle A\rangle$ from the time series of observations of $A(r)$ or a related observable $\tilde{A}(r,s)$ during the dAFED simulation. In the Appendix, we show that this is impractical, because the appropriate expression for the observable $\tilde{A}(r,s)$ contains the PMF $\tilde{\phi}_\beta(s)$, which is unknown until the end of the simulation.

The TI-dAFED Method. An alchemical transformation from a first system described by Hamiltonian $H_A(r,p)$ to a second system described by $H_B(r,p)$ can be described by a

dx.doi.org/10.1021/ct300090z | J. Chem. Theory Comput. XXXX, XXX, XXX−XXX

hybrid Hamiltonian $H(r,p;\lambda)$ depending on a parameter λ, such that $H(r,p;0) = H_A(r,p)$ and $H(r,p;1) = H_B(r,p)$. If we are interested in the free energy difference $\Delta F_{AB} = F_B - F_A$, the functional form of the λ interpolation in $H(r,p;\lambda)$ is arbitrary. According to the TI method[4]

$$\Delta F_{AB} = \int_0^1 \mathrm{d}\lambda \left\langle \frac{\partial H}{\partial \lambda} \right\rangle (\lambda) \tag{17}$$

Here, $\langle\cdot\rangle(\lambda)$ indicates an ensemble average for the hybrid system $H(r,p;\lambda)$ with fixed λ. In practice, we perform a number of simulations with λ values chosen at discrete intervals between 0 and 1, which we call λ points. During each simulation, we accumulate the average of the observable $A = \partial H/\partial\lambda$. In a post processing stage, the integral in eq 17 is performed numerically.

As outlined in the Introduction, it was recognized very early[9,10] that the convergence of $\langle\cdot\rangle(\lambda)$ might be hindered by free energy barriers in the conformational space. Here, we propose to use the dAFED method summarized above to accelerate the convergence of eq 17. The first step is to choose a set of CVs, $q(r) \equiv (q_1(r),...,q_n(r))$. Note that the CVs should be chosen primarily on their ability to drive the system most efficiently across high conformational free energy barriers. Indeed, interpreting the resulting PMF is secondary, as it is only an auxiliary quantity for the alchemical free energy calculation.

For each λ point, we then run a dAFED simulation with extended variables $s \equiv (s_1,...,s_n)$ coupled to the corresponding CVs. We accumulate either the histogram $\rho_{\mathrm{adb}}(s;\lambda)$ or the mean force $\langle f\rangle_r(s;\lambda)$ in bins covering the space of s. In the same bins, we collect the local average $\langle \partial H/\partial\lambda\rangle_r(s;\lambda)$ defined by eq 14 with observable $A = \partial H/\partial\lambda$. To keep the notation simple, we omit the subscript β in this section, but it should be emphasized that both $\langle \partial H/\partial\lambda\rangle_r(s;\lambda)$ and $\tilde{\phi}(s;\lambda)$ correspond to the system at temperature T, although the actual simulation is performed with the extended variables at temperature T_s.

In a postprocessing stage, we use eq 7 or eq 11 to obtain the PMF $\tilde{\phi}(s;\lambda)$. Then, we integrate eq 16 numerically, for each λ point, to get

$$\left\langle \frac{\partial H}{\partial \lambda} \right\rangle (\lambda) = \frac{1}{\tilde{Z}(\lambda)} \int \mathrm{d}s \left\langle \frac{\partial H}{\partial \lambda} \right\rangle_r (s;\lambda)\, \mathrm{e}^{-\beta\tilde{\phi}(s;\lambda)} \tag{18}$$

where $\tilde{Z}(\lambda) = \int \mathrm{d}s\, \mathrm{e}^{-\beta\tilde{\phi}(s;\lambda)}$. The last step is to use eq 17 to calculate the overall free energy variation ΔF_{AB} by integrating the result of eq 18 over λ.

The profile of $\langle \partial H/\partial\lambda\rangle_r(s;\lambda)$ in the CV space might be interesting *per se*, as it holds information about which conformations contribute to the free energy change. It is tempting to go one step further by inverting the order of the integrations over s and over λ in eqs 17 and 18 to find an expression for the *local* contribution to the total free energy change

$$\Delta F_{AB}(s) = \int_0^1 \mathrm{d}\lambda \left\langle \frac{\partial H}{\partial \lambda} \right\rangle_r (s;\lambda) \frac{\mathrm{e}^{-\beta\tilde{\phi}(s;\lambda)}}{\tilde{Z}(\lambda)} \tag{19}$$

As we will see in the Results section, however, $\Delta F_{AB}(s)$ is not a state function. But for a given λ path, the associated maps over the CV space can be used to interpret which conformations of a ligand contribute most to the binding free energy difference.

The FEP-dAFED Method. We consider again an alchemical transformation described by a hybrid Hamiltonian of the form $H(r,p;\lambda)$ defined as above, with m λ-points covering the interval $[0,1]$. According to the FEP method, the free energy difference between system A and system B can be calculated with

$$\Delta F_{AB} = -\sum_{i=1}^{m-1} \frac{1}{\beta} \ln\langle \mathrm{e}^{-\beta\Delta H_i}\rangle(\lambda_i) \tag{20}$$

Here, $\langle\cdot\rangle(\lambda_i)$ is the ensemble average with $\lambda = \lambda_i$ fixed and $\Delta H_i(r) = H(r,p;\lambda_{i+1}) - H(r,p;\lambda_i)$. Note that because the dependence on λ appears only in the potential energy function, $\Delta H_i(r)$ is a function of positions only. Thus, eq 20 amounts to evaluating the ensemble average of the FEP observable $A(r) = \mathrm{e}^{-\beta\Delta H_i(r)}$. Due to the strong decay of the exponential function, λ points should be chosen to be sufficiently close so that ΔH_i is never much larger than k_BT. In other words, FEP is most effective when the distributions of states for λ_i and λ_{i+1} have sufficient overlap.

If significant conformational free energy barriers are present in the system, we can choose a set of CVs and perform a dAFED simulation at each λ point as outlined above. In each simulation, we accumulate the local average $\langle \mathrm{e}^{-\beta\Delta H_i}\rangle_r(s;\lambda_i)$, as defined in eq 14. We also calculate the PMF $\tilde{\phi}(s;\lambda_i)$ using either eq 7 or eq 11. Then, we use eq 16 to integrate over the CV space and recover the overall ensemble average $\langle \mathrm{e}^{-\beta\Delta H_i}\rangle(\lambda_i)$ for each λ point. We finally insert the results back into eq 20 to yield

$$\Delta F_{AB} = -\sum_{i=1}^{m-1} \frac{1}{\beta} \ln\left[\frac{1}{\tilde{Z}(\lambda_i)} \int \mathrm{d}s\, \langle \mathrm{e}^{-\beta\Delta H_i}\rangle_r(s;\lambda_i) \mathrm{e}^{-\beta\tilde{\phi}(s;\lambda_i)} \right] \tag{21}$$

It is important to realize that, although β_s does not appear in eq 21, the simulation is performed with extended variables at temperature T_s. Note that, due to the presence of the logarithm in eq 21, it is not possible to invert the summation over λ points and the integration over s to obtain an expression similar to eq 19 for the local contribution $\Delta F_{AB}(s)$ in the FEP framework.

SIMULATION RESULTS

Toy Problem. We consider the two-dimensional potential energy function

$$V(x,y) = D_0(x^2 - 1)^2 + \frac{1}{2}\kappa y^2 + \lambda xy \tag{22}$$

previously used to validate the AFED and dAFED methods.[36,33] By analytically integrating the partition function over y with inverse temperature $T = 1.0$ (for this example, we set $k_B = 1$), we obtain the PMF along x

$$\phi(x) = D_0(x^2 - 1)^2 - \frac{\lambda^2}{2\kappa}x^2 \tag{23}$$

This PMF has a barrier at $x = 0$ and symmetrical minima at $x_\pm = \pm(1 + \lambda^2/4D_0\kappa)^{1/2}$. The resulting barrier height is $F^\ddagger = F(0) - F(x_\pm) = D_0 + \lambda^2/2\kappa + \lambda^4/16D_0\kappa^2$.

Numerically integrating $\mathrm{e}^{-\beta\phi(x)}$ over x yields a theoretical value for the free energy $F(\lambda)$ of the system for a given value of the parameter λ. To validate the TI-dAFED method, we propose to calculate via MD the variation of $F(\lambda)$ upon increasing λ from 2.0 to 3.0, $\Delta F_{2\to3} = F(3.0) - F(2.0)$.

We set $\kappa = 1.0$, $m = 1.0$, and $D_0 = 5.0$. With these values, $F^\ddagger = 7.2$ for $\lambda = 2.0$ and $F^\ddagger = 10.5$ for $\lambda = 3.0$, such that barrier crossing is a rare event using standard NVT dynamics at temperature $T = 1.0$. To enhance sampling, we choose $q(x,y) =$

dx.doi.org/10.1021/ct300090z | J. Chem. Theory Comput. XXXX, XXX, XXX−XXX

x as the CV and couple it with harmonic constant k = 1000 to the dAFED extended variable s with mass m_s = 1000 and temperature T_s = 5. We use a time step $\Delta t = 10^{-3}$ and couple each degree of freedom to a generalized Gaussian moment thermostat (GGMT)[40] of order 2. For the TI calculation we choose to estimate $\langle \partial H/\partial\lambda \rangle(\lambda)$ for 11 values of λ separated by intervals of 0.1 between λ = 2.0 and λ = 3.0.

The TI-dAFED results are shown in Figure 1. For clarity we show only the curves corresponding to simulations at λ = 2.0 and λ = 3.0. Panel a shows that the PMFs obtained via eq 7 correctly reproduce the theoretical PMFs from eq 23, as expected from ref 33. Panel b shows the integrand in eq 18, namely, $\langle \partial H/\partial\lambda \rangle(s;\lambda)\ e^{-\beta\tilde{\phi}(s;\lambda)}$. This quantity indicates which domains of the CV space participate most in the change in free energy. The small discrepancies between analytical and simulation data do not seem to impact significantly the final free energy difference.

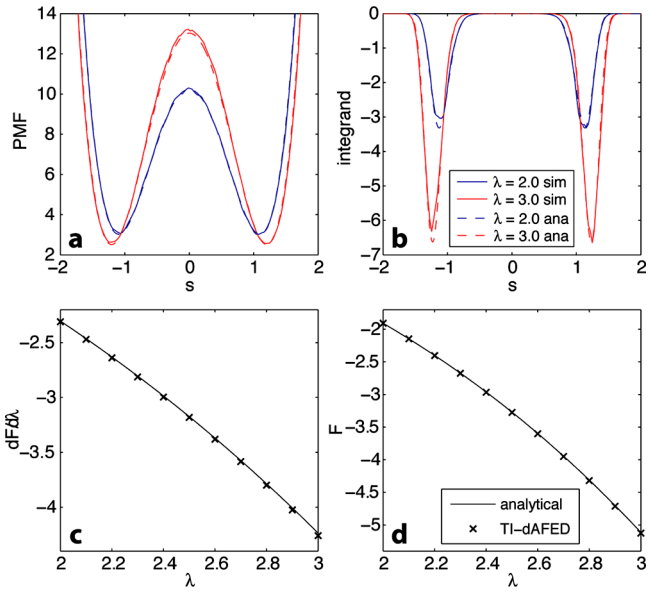

Figure 1. Numerical results for the two-dimensional toy problem described by eq 22. (a) PMFs for λ = 2.0 and λ = 3.0. The dashed lines represent the analytical results from eq 23, and plain lines represent simulation results. (b) Integrand of eq 18 as a function of the CV s. (c) Free energy derivatives for different values of λ. (d) Free energy variation as a function of λ. In panels c and d, crosses represent TI-dAFED results calculated using eqs 18 and 17; the line represents analytical results.

In Figure 1, panel c shows the free energy derivatives evaluated using eq 18 from the simulations at each λ point, which perfectly match with the analytical result. Finally, panel d shows the free energy variation obtained by integrating eq 17 numerically from 0 to λ. For the simulation results, the integration constant has been set such that $F(2.0)$ matches the theoretical value. The statistical error was estimated with the bootstrap method[41] acting on 200 blocks of trajectory data. The resulting 95% confidence intervals on both $dF/d\lambda$ and F were too small to be reported in Figure 1.

The final result is $\Delta F_{2\to3} = -3.217 \pm 0.004$, in good agreement with the theoretical value of −3.206, although the statistical error does not account for the entire discrepancy. The very small residual systematic error is attributable to numerical drift in the molecular dynamics algorithm or to imperfect adiabaticity in the dAFED simulations. With this toy example, we have verified that the TI-dAFED method is valid. In particular, we have shown that ensemble averages can be computed accurately for a dynamical system at temperature T using an extended variable at temperature $T_s = 5T$.

Alanine Dipeptide Enantiomerization in Explicit Solvent. The next step in validating the TI-dAFED and FEP-dAFED methods is to apply them to a simple molecular system. We need an alchemical transformation for which the free energy difference is known *a priori*. We propose to calculate the enantiomerization free energy of the alanine dipeptide (N-acetyl-Ala-methylamide) in solution. Going from L-Ala to D-Ala should result in a free energy change $\Delta F_{L\to D} = 0$. The natural choice of CVs for this system is the two backbone dihedral angles Φ and Ψ.

The alchemical transformation gradually decouples the L-Ala methyl side chain, while another methyl group is simultaneously grown at the location of the D-Ala side chain. For comparison, we performed two calculations with different λ paths interpolating the corresponding Hamiltonians. In the first calculation, each force field parameter is linearly interpolated from one topology (L-Ala) to the other (D-Ala). The second calculation uses soft-core potentials[30] for the methyl side chains. The soft-core potentials avoid singularities at the center of vanishing atoms and thus produce smoother derivatives of the Hamiltonian close to λ = 0 or λ = 1.

The system is modeled with the Gromos 53a6 united atom force field[42] and placed in a periodic box of 1009 explicit SPC water molecules.[43] We used the software Gromacs version 4.5.3[44] with standard settings for the Gromos force field. For nonbonded interactions, a twin range scheme is used with short-range interactions up to 0.9 nm updated every time step and long-range interactions up to 1.4 nm updated every five steps. The nonbonded interactions smoothly reach zero at the cutoff thanks to a shift for the Lennard-Jones potential and a reaction field correction[45] for the Coulomb term. All bonds were constrained, and a time step of 2 fs was used. Protein and solvent were coupled to heat baths at 300 K using Nosé–Hoover chain[46] thermostats. A standard equilibration protocol was followed, including a heat-up phase, an NPT equilibration, and an NVT equilibration for a total of 1.3 ns. The dAFED algorithm was implemented in a modified version of the PLUMED plugin[47] version 1.2.2. Note that our dAFED implementation is now part of the present PLUMED 1.3 release.

The λ values were chosen at regular intervals of 0.05 between 0 and 1. Because the free energy derivative changes abruptly close to the end points with the linear interpolation scheme (see Figure 3), additional trajectories were run with λ values at 0.001, 0.01, and 0.02 and at 0.98, 0.99, and 0.999. For each λ value, a 50 ns NVT dAFED simulation was performed with extended variables s_1 and s_2 coupled to the dihedral angles Φ and Ψ and maintained at temperature T_s = 1200 K by GGMT thermostats[40] with a time constant of 0.1 ps. As the coupling constant k controls the spatial resolution of the resulting PMF, the highest value should be chosen (k = 1000 kJ/mol/rad^2), for which the resulting force can still be integrated accurately given the MD time step. This can be checked by inspecting a short preliminary trajectory segment in which data were saved very frequently. Both extended variables are assigned a fictitious mass m_s = 500 amu·nm^2/rad^2. As in regular dAFED simulations, m_s is chosen as large as possible for the best adiabatic separation, but small enough to allow sufficient sampling of the CV space during the planned simulation time.

dx.doi.org/10.1021/ct300090z | J. Chem. Theory Comput. XXXX, XXX, XXX−XXX

Note that the units of k and m_s must be such that ks^2 and $m_s\dot{s}^2$ have units of energy.

As an *a posteriori* consistency check, we verify that the distribution of kinetic temperature in the peptide conforms with the canonical ensemble at 300 K, see Figure S1 in the Supporting Information. To further assess the adiabatic separation, we ran dAFED simulations at the first λ point with m_s ranging from 0.1 to 5000 amu·nm^2/rad^2; we observed that the average work that the extended variables exert on the physical system decreases as $m_s^{-0.89}$, see Figure S2 in the Supporting Information. Above m_s = 50 amu·nm^2/rad^2, the numerical value of $\langle \partial H/\partial\lambda \rangle$ is robust to variations of m_s, within error bars.

Figure 2 shows the PMFs in the (Φ,Ψ) plane obtained for selected λ points along the linearly interpolated path. The D-Ala dipeptide (λ = 1.0) closely resembles the PMF of the usual L-Ala dipeptide (λ = 0.0) with the signs of Φ and Ψ inverted. The same symmetry is apparent between the λ = 0.2 and λ = 0.8 PMFs. The value λ = 0.5 corresponds to a symmetric hybrid molecule with one half-coupled methyl side chain on each side of the backbone. As expected, the corresponding PMF is almost invariant under a 180° rotation. The general consistency of the PMFs across the range of λ ensures that simulations have reached acceptable convergence.

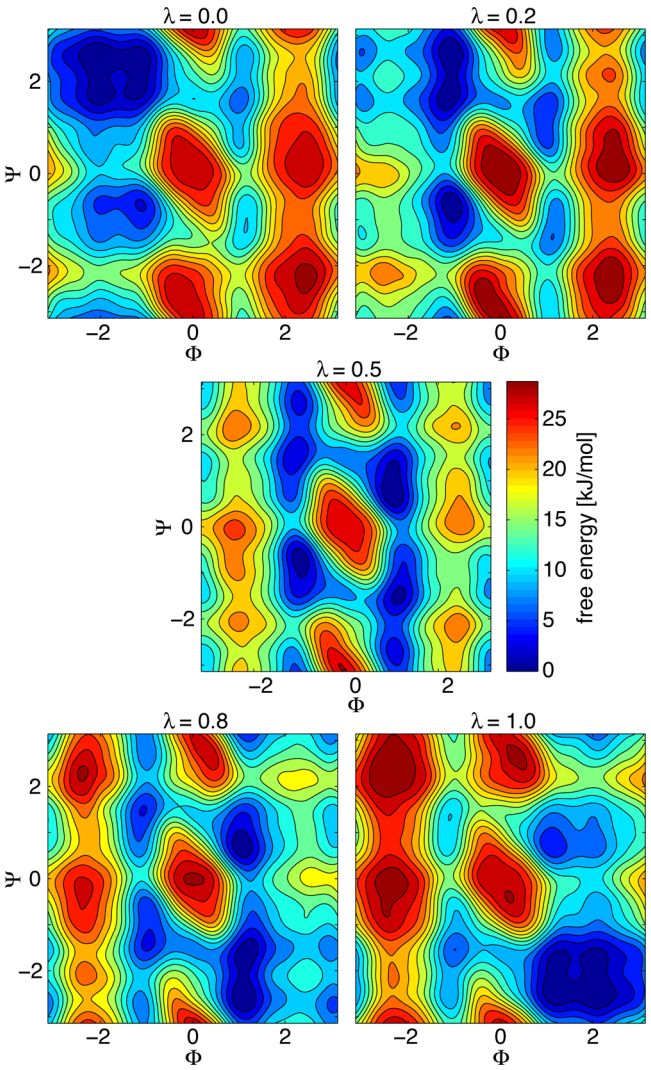

Figure 2. PMFs for the alanine dipeptide in solution, at selected values of λ along the linearly interpolating λ path. Here, λ = 0.0 represents L-Ala and λ = 1.0 represents D-Ala.

For each λ point, the TI-dAFED free energy derivatives were accumulated in 100 × 100 bins uniformly covering the (Φ, Ψ) plane. In the same bins, the mean force, eq 10, was obtained, and the PMF was calculated using eq 11. Both the PMF and the free energy derivatives were smoothed in the (Φ, Ψ) plane using a robust spline algorithm.[48] Finally, the mean alchemical force at each λ point was calculated using eq 18. Results are shown in panels a and d of Figure 3. The error bars represent 95% confidence intervals obtained using the bootstrapping method with 200 trajectory segments. Panel a, corresponding to the linear λ path, shows sharp variations close to the end points, as expected, which justifies the choice of close-set λ points. The soft-core λ path yields a smoother $\partial F/\partial\lambda$ (λ) function well captured by fewer, evenly spaced λ points.

The thermodynamic integration results of eq 17 with integration interval [0,λ] are shown on panels b and e of Figure 3, which also show the FEP-dAFED results obtained from the same simulations using eq 21. For the linear λ path (Figure 3e), the final results are $\Delta F_{L\to D}$ = −0.19 ± 0.34 kJ/mol for TI-dAFED and $\Delta F_{L\to D}$ = −0.03 ± 0.34 for FEP-dAFED, in good agreement with the expected value of zero. At intermediate λ points, the FEP-dAFED free energy profile is slightly less prominent than the TI-dAFED one (up to 0.48 kJ/mol difference at intermediate λ points). Closer inspection reveals that the difference between free energy curves builds up at the first λ points up to λ = 0.02 then remains approximately constant up to λ = 0.98, where it starts to decrease again. This shows that TI-dAFED and FEP-dAFED are affected differently in regions where the free energy curve is steep but does not indicate which method is most accurate. Regardless, the precision of the methods, within 0.5 kJ/mol, is already satisfactory for practical applications.

With the soft-core λ path, large values of $\langle \partial H/\partial\lambda \rangle$ are avoided, and the difference between TI-dAFED and FEP-dAFED becomes negligible relative to the error bars, see Figure 3e. The resulting final free energy differences, $\Delta F_{L\to D}$ = −0.14 ± 0.29 kJ/mol for TI-dAFED and $\Delta F_{L\to D}$ = −0.11 ± 0.30 kJ/mol for FEP-dAFED are in excellent agreement with the expected value of zero.

Parts c and f of Figure 3 show maps in the (Φ,Ψ) plane of the contributions to $\Delta F_{L\to D}$, as obtained with eq 19. Not surprisingly, contributions are symmetrical for the enantiomerization reaction. The maps clearly differ between both λ paths, which demonstrates that $\Delta F_{L\to D}(s)$ given by eq 19 is not a state function. This prevents us from using maps such as those shown in Figure 3c and f to predict which conformations contribute most to the final free energy difference in general. However, these maps could provide indications toward optimizing the λ path. Finally, the maps clearly show that various conformations contribute to $\Delta F_{L\to D}$, which confirms that efficient conformational sampling is key to the fast convergence of the alchemical free energy difference.

CONCLUSION

Our central theoretical result is eq 16, which establishes that ensemble averages of any observable depending on the physical system's coordinates can be obtained from a dAFED simulation. As an application, we have shown that thermodynamic integration or free energy perturbation can be combined with the dAFED method to enhance conformational sampling

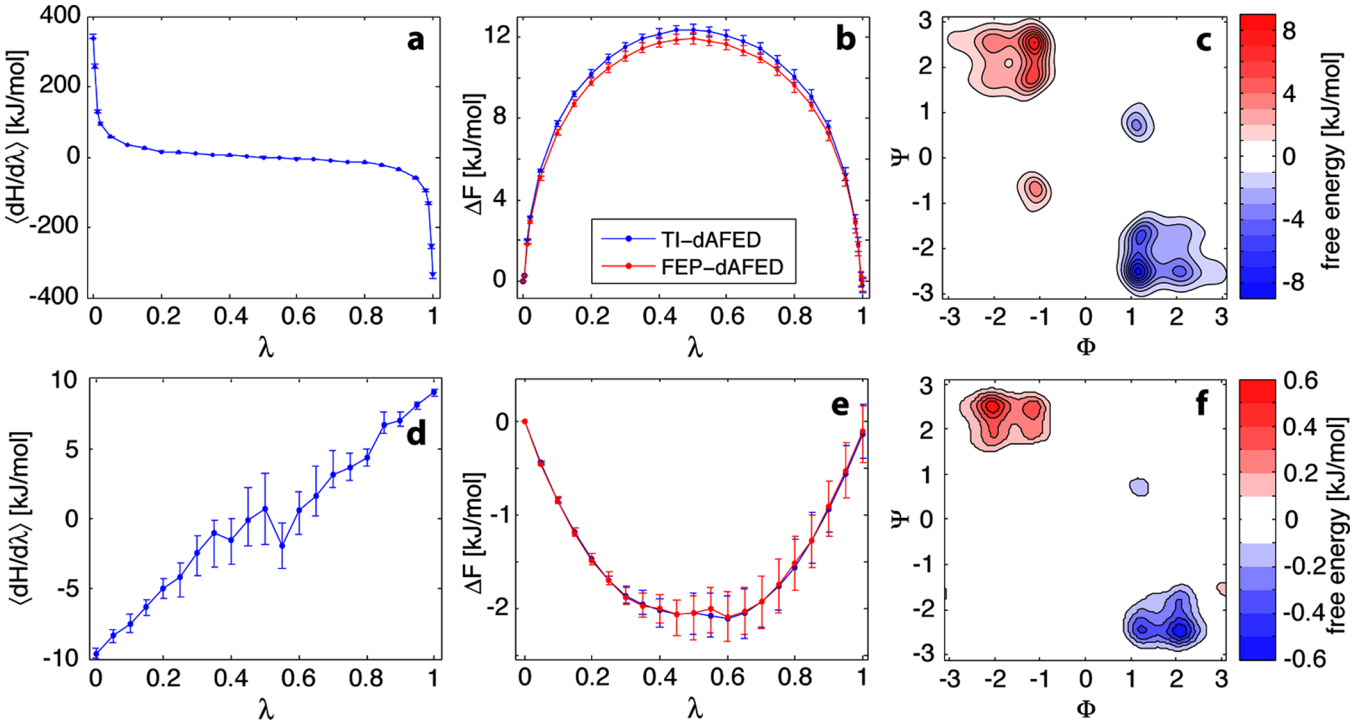

Figure 3. Alchemical free energy results for the enantiomerization of the alanine dipeptide in solution using the linearly interpolated λ path (upper row) or soft-core potentials (lower row). (a and d) Derivatives of the free energy for TI-dAFED obtained with eq 18. (b and e) Free energy profile calculated with eq 17 for TI-dAFED (blue) and with eq 21 for FEP-dAFED (red). (c and f) Contribution to the alanine dipeptide enantiomerization free energy as a function of the backbone dihedral angles, as calculated with eq 19.

and speed up alchemical free energy simulations. We have provided a proof of principle of the method by simulating a two-dimensional system with a known theoretical solution. We have also shown the applicability of TI-dAFED and FEP-dAFED to a realistic molecular system by correctly reproducing the zero free energy change associated with the enantiomerization of the alanine dipeptide in solution.

What mainly differentiates TI-dAFED and FEP-dAFED from existing enhanced sampling methods for alchemical free energy simulations is the fact that they rely on the definition of CVs. The choice of these CVs is both arbitrary and important for the efficiency of the simulation. In addition, the number of these CVs is limited to three or four with the original implementations of dAFED (this number could be increased by a few units with the recent force-based dAFED method[34]). Therefore, at first sight, the requirement to choose CVs can be seen as a limit to the generality of the TI-dAFED and FEP-dAFED methods. However, in the cases where the nature of the free energy barriers is known, defining CVs is easy, and the method can confer some desirable advantages. First, enhanced sampling can be focused on the particular degrees of freedom problematic for the alchemical transformation, which is often localized on a few atoms in the system. Second, obtaining the PMFs of both molecules A and B as a byproduct can bring valuable insight on, e.g., how the binding modes of two drug candidates differ.

Further developments of the TI-dAFED and FEP-dAFED methods are under way. These include using the recent improvements of the dAFED method, in which an adaptive bias potential is introduced to dramatically improve the sampling efficiency.[34] Beyond the TI and FEP approaches, we expect that combining TAMD/dAFED with λ dynamics approaches such as λ-AFED[26] will yield additional improvements in efficiency. The ability to calculate ensemble averages of any observable from a dAFED simulation immediately suggests combining dAFED with other alchemical free energy methods such as the efficient Bennett acceptance ratio method.[49] On the other hand, other CV-based enhanced sampling methods such as metadynamics[50] or adaptive biasing force[51] could be combined with alchemical free energy methods, based on relationships equivalent to eq 16 to recover the correct ensemble averages from modified CV distributions. More work is also necessary to assess the efficiency of TI-dAFED and FEP-dAFED in biologically relevant applications, such as solvation free energy differences of flexible ligands, which are necessary ingredients for the computation of accurate binding free energies.

APPENDIX

At the end of the Methodology section, we raised the question of whether one could obtain $\langle A \rangle$ from the time series of observations of $A(r)$ during the dAFED simulation. Using the ergodic hypothesis, the resulting time average would be equivalent to

$$\langle A \rangle_{\mathrm{adb}} = \frac{\int \mathrm{d}s\, \langle A \rangle_r(s)\, \mathrm{e}^{-\beta_s \tilde{\phi}_\beta(s)}}{\int \mathrm{d}s\, \mathrm{e}^{-\beta_s \tilde{\phi}_\beta(s)}} \tag{24}$$

Comparing to the definition of $\langle A \rangle$, eq 16, we see that $\langle A \rangle_{\mathrm{adb}} \neq \langle A \rangle$, due to the different inverse temperatures in the Boltzmann weights. Could we sample a modified observable $\tilde{A}$, such that $\langle \tilde{A} \rangle_{\mathrm{adb}} = \langle A \rangle$ and the time average would yield the correct answer? Comparing eq 16 and eq 24, we see that

$$\tilde{A}(r,s) = \frac{\tilde{Z}_{\beta_s}}{\tilde{Z}_\beta} A(r)\, \mathrm{e}^{-[\beta-\beta_s]\tilde{\phi}_\beta(s)} \tag{25}$$

dx.doi.org/10.1021/ct300090z | J. Chem. Theory Comput. XXXX, XXX, XXX−XXX

This is an impractical observable, because it depends on the whole PMF. Evaluating such an observable would imply first performing a separate dAFED simulation to calculate the PMF, before running a second simulation to accumulate the time average of $\tilde{A}$. Therefore, in most cases, the best way to calculate an ensemble average is using eq 16 and a numerical integration scheme.

■ ASSOCIATED CONTENT

Supporting Information

Figure S1 shows the kinetic temperature distribution in the alanine dipeptide during a TI-dAFED simulation. Figure S2 shows the work exerted by the extended variables during TI-dAFED simulations with different masses, as well as the robustness of the $\langle \partial H/\partial \lambda \rangle$ values obtained in these simulations. This information is available free of charge via the Internet at http://pubs.acs.org

■ AUTHOR INFORMATION

Corresponding Author

*E-mail: mark.tuckerman@nyu.edu.

Notes

The authors declare no competing financial interest.

■ ACKNOWLEDGMENTS

This work has been funded by the Advanced Researcher Fellowship PA00P2_129092 of the Swiss National Science Foundation for M.A.C and the U.S. National Science Foundation grant CHE-1012545 for M.E.T. Computing resources were provided by the Vital-IT infrastructure of the Swiss Institute of Bioinformatics. We are grateful to M. Chen for insightful discussions and to T. Purcell and D. Margul for proofreading the manuscript.

■ DEDICATION

It is our privilege to participate in this JCTC special issue dedicated to W. F. van Gunsteren, and we salute his tremendous contribution to the field. M.A.C. takes the opportunity to express his sincere gratitude for the great time he spent as a Ph.D. student in W. F. van Gunsteren's group.

■ REFERENCES

(1) van Gunsteren, W. F.; Daura, X.; Mark, A. E. *Helv. Chim. Acta* **2002**, *85*, 3113−3129.
(2) Chipot, C.; Pohorille, A. *Free Energy Calculations, Theory and Applications in Chemistry and Biology*; Springer: Berlin, 2007; Springer Series in Chemical Physics, Vol. *86*.
(3) Tembe, B. L.; McCammon, J. A. *Comput. Chem.* **1984**, *8*, 281−283.
(4) Kirkwood, J. G. *J. Chem. Phys.* **1935**, *3*, 300−313.
(5) Zwanzig, R. W. *J. Chem. Phys.* **1954**, *22*, 1420−1426.
(6) Chodera, J. D.; Mobley, D. L.; Shirts, M. R.; Dixon, R. W.; Branson, K.; Pande, V. S. *Curr. Opin. Struct. Biol.* **2011**, *21*, 150−160.
(7) Christ, C.; Mark, A.; Van Gunsteren, W. *J. Comput. Chem.* **2010**, *31*, 1569−1582.
(8) Simonson, T.; Archontis, G.; Karplus, M. *Acc. Chem. Res.* **2002**, *35*, 430−437.
(9) Straatsma, T. P.; McCammon, J. A. *J. Chem. Phys.* **1989**, *90*, 3300−3304.
(10) Tobias, D.; Brooks, C., III; Fleischman, S. *Chem. Phys. Lett.* **1989**, *156*, 256−260.
(11) Lawrenz, M.; Baron, R.; McCammon, J. *J. Chem. Theory Comput.* **2009**, *5*, 1106−1116.
(12) Lawrenz, M.; Baron, R.; Wang, Y.; McCammon, J. *J. Chem. Theory Comput.* **2011**, *7*, 2224−2232.
(13) Zagrovic, B.; van Gunsteren, W. F. *J. Chem. Theory Comput.* **2007**, *3*, 301−311.
(14) Mobley, D.; Chodera, J.; Dill, K. *J. Chem. Theory Comput.* **2007**, *3*, 1231−1235.
(15) Verkhivker, G.; Elber, R.; Nowak, W. *J. Chem. Phys.* **1992**, *97*, 7838−7841.
(16) Woods, C.; Jonathan, W.; King, M. *J. Phys. Chem. B* **2003**, *107*, 13703−13710.
(17) Min, D.; Li, H.; Li, G.; Bitetti-Putzer, R.; Yang, W. *J. Chem. Phys.* **2007**, *126*, 144109.
(18) Li, H.; Fajer, M.; Yang, W. *J. Chem. Phys.* **2007**, *126*, 024106.
(19) Meng, Y.; Sabri Dashti, D.; Roitberg, A. *J. Chem. Theory Comput.* **2011**, *7*, 2721−2727.
(20) Jiang, W.; Hodoscek, M.; Roux, B. *J. Chem. Theory Comput.* **2009**, *5*, 2583−2588.
(21) Jiang, W.; Roux, B. *J. Chem. Theory Comput.* **2010**, *6*, 2559−2565.
(22) Kong, X.; Brooks, C., III. *J. Chem. Phys.* **1996**, *105*, 2414−2423.
(23) Bitetti-Putzer, R.; Yang, W.; Karplus, M. *Chem. Phys. Lett.* **2003**, *377*, 633−641.
(24) Knight, J.; Brooks, C., III. *J. Comput. Chem.* **2009**, *30*, 1692−1700.
(25) Torrie, G. M.; Valleau, J. P. *J. Comput. Phys.* **1977**, *23*, 187−199.
(26) Abrams, J.; Rosso, L.; Tuckerman, M. *J. Chem. Phys.* **2006**, *125*, 074115.
(27) Wu, P.; Hu, X.; Yang, W. *J. Phys. Chem. Lett.* **2011**, *2*, 2099−2103.
(28) Leitgeb, M.; Schröder, C.; Boresch, S. *J. Chem. Phys.* **2005**, *122*, 084109.
(29) Hritz, J.; Oostenbrink, C. *J. Phys. Chem. B* **2009**, *113*, 12711−12720.
(30) Beutler, T. C.; Mark, A. E.; van Schaik, R. C.; Gerber, P. B.; van Gunsteren, W. F. *Chem. Phys. Lett.* **1994**, *222*, 529−539.
(31) de Oliveira, C. A. F.; Hamelberg, D.; McCammon, J. A. *J. Chem. Theory Comput.* **2008**, *4*, 1516−1525.
(32) Maragliano, L.; Vanden-Eijnden, E. *Chem. Phys. Lett.* **2006**, *426*, 168−175.
(33) Abrams, J. B.; Tuckerman, M. E. *J. Phys. Chem. B* **2008**, *112*, 15742−15757.
(34) Chen, M.; Cuendet, M. A.; Tuckerman, M. E. *J. Chem. Phys.* **2012**, *137*, 024102.
(35) Maragliano, L.; Vanden-Eijnden, E. *J. Chem. Phys.* **2008**, *128*, 184110.
(36) Rosso, L.; Minary, P.; Zhu, Z.; Tuckerman, M. E. *J. Chem. Phys.* **2002**, *116*, 4389−4402.
(37) Rosso, L.; Tuckerman, M. E. *Mol. Simul.* **2002**, *28*, 91−112.
(38) Rosso, L.; Abrams, J. B.; Tuckerman, M. E. *J. Phys. Chem. B* **2005**, *109*, 4162−4167.
(39) VandeVondele, J.; Roethlisberger, U. *J. Phys. Chem. B* **2002**, *106*, 203−208.
(40) Liu, Y.; Tuckerman, M. E. *J. Chem. Phys.* **2000**, *112*, 1685−1700.
(41) Davison, A.; Hinkley, D. *Bootstrap Methods and Their Application*; Cambridge University Press: New York, 1997.
(42) Oostenbrink, C.; Villa, A.; Mark, A. E.; van Gunsteren, W. F. *J. Comput. Chem.* **2004**, *25*, 1656−1676.
(43) Berendsen, H. J. C.; Postma, J. P. M.; van Gunsteren, W. F.; Hermans, J. In *Intermolecular Forces*; Pullman, B., Ed.; Reidel: Dordrecht, The Netherlands, 1981; p 331.
(44) Hess, B.; Kutzner, C.; van der Spoel, D.; Lindahl, E. *J. Chem. Theory Comput.* **2008**, *4*, 435−447.
(45) Tironi, I.; Sperb, R.; Smith, P.; van Gunsteren, W. *J. Chem. Phys.* **1995**, *102*, 5441−5459.
(46) Martyna, G. J.; Klein, M. L.; Tuckerman, M. *J. Chem. Phys.* **1992**, *97*, 2635−2643.
(47) Bonomi, M.; Branduardi, D.; Bussi, G.; Camilloni, C.; Provasi, D.; Raiteri, P.; Donadio, D.; Marinelli, F.; Pietrucci, F.; Broglia, R.; Parrinello, M. *Comput. Phys. Commun.* **2009**, *180*, 1961−1972.

(48) Garcia, D. *Comput. Stat. Data Anal.* **2010**, *54*, 1167−1178.
(49) Bennett, C. H. *J. Comput. Phys.* **1976**, *22*, 245−268.
(50) Laio, A.; Parrinello, M. *Proc. Natl. Acad. Sci. U.S.A.* **2002**, *99*, 12562−12566.
(51) Darve, E.; Wilson, M. A.; Pohorille, A. *Mol. Simul.* **2002**, *28*, 113−144.